Available online at www.sciencedirect.com
SCIENCE DIRECT®
International Journal of Plasticity 21 (2005) 2319–2343
INTERNATIONAL JOURNAL OF Plasticity
www.elsevier.com/locate/ijplas

Continuous, large strain, tension/compression testing of sheet material

R.K. Boger [a], R.H. Wagoner [a,*], F. Barlat [b], M.G. Lee [c], K. Chung [c]

[a] *Ohio State University, Department of Materials Science and Engineering, 477 Watts Hall, 2041 College Road, Columbus, OH 43210, USA*
[b] *Materials Science Division, Alcoa Technical Center, 100 Technical Drive, Alcoa Center, PA 15069-0001, USA*
[c] *Seoul National University, School of Materials Science and Engineering, 56-1 Shinlim-dong, Kwanak-gu, Seoul 151-742, Korea*

Received 5 September 2004
Available online 24 May 2005

Abstract

Modeling sheet metal forming operations requires understanding of the plastic behavior of sheet alloys along non-proportional strain paths. Measurement of hardening under reversed uniaxial loading is of particular interest because of its simplicity of interpretation and its application to material elements drawn over a die radius. However, the compressive strain range attainable with conventional tests of this type is severely limited by buckling. A new method has been developed and optimized employing a simple device, a special specimen geometry, and corrections for friction and off-axis loading. Continuous strain reversal tests have been carried out to compressive strains greater than 0.20 following the guidelines provided for optimizing the test. The breadth of application of the technique has been demonstrated by preliminary tests to reveal the nature of the Bauschinger effect, room-temperature creep, and anelasticity after strain reversals in commercial sheet alloys.
© 2005 Elsevier Ltd. All rights reserved.

* Corresponding author. Tel.: +1 614 292 2079; fax: +1 614 292 6530.
E-mail address: wagoner.2@osu.edu (R.H. Wagoner).

0749-6419/$ - see front matter © 2005 Elsevier Ltd. All rights reserved.
doi:10.1016/j.ijplas.2004.12.002

Keywords: Mechanical testing; Bauschinger effect; Tension/compression testing; Anelasticity; Room temperature creep; Aluminum alloys; Steel; Magnesium; Zinc

1. Introduction

The fact that a material's mechanical properties depend on its loading path has been well known for over a century from the work of Johann Bauschinger (Bauschinger, 1886). Bauschinger's results showed that the yield stress of mild steel is lowered by prior strain in a direction opposite of the testing direction. Subsequent phenomenological and microstructural descriptions of the Bauschinger effect have been concerned not only with the initial reverse yield point, but with the entire stress–strain response after reversal. Review articles have appeared describing the Bauschinger effect for many materials (Sowerby et al., 1979; Bate and Wilson, 1986; Abel, 1987).

In recent years, there has been renewed emphasis on understanding mechanical behavior under non-proportional paths as it relates to simulating forming processes. Simple material models, such as isotropic hardening, are not sufficient to predict springback of formed parts after removal from a die (Li et al., 2002). Because of the need for more refined constitutive relations, many new continuum and physical models have been developed to describe materials that undergo load reversals (Chaboche, 1989; Geng, 2000; Chun et al., 2002; Geng and Wagoner, 2002; Kang et al., 2003; Colak, 2004). In order to fit these new constitutive equations, experimental methods are required to test materials under non-proportional loading in an accurate, reliable and reproducible manner.

Several methods have been developed to test materials along reverse loading paths. Reverse torsion (Hill, 1948; Stout and Rollett, 1990; Anand and Kalidindi, 1994; Chen et al., 1999) or a combination of torsion and tension (Brown, 1970) has been used, with strains approaching 6.0 possible with appropriate samples (Stout and Rollett, 1990). Sheet material can be tested using torsion methods by welding the sheet into a thin-walled tube. However, rolling and welding the sheet to form the tube can change the structure of the sheet, thus altering its macroscopic properties. Another disadvantage of torsion testing is that stress and strain are not uniform throughout the cross section of the sample, requiring the strain gradient in the radial direction to be taken into account (Wu et al., 1996). The presence of this gradient creates fundamental problems in constitutive equation development because the transformation of the torque/twist data to shear-stress/shear-strain curves is indefinite if the reverse loading curve varies with prestrain as shown by Geng et al. (2002) for reverse-bend tests.

The Bauschinger effect has been studied through reverse shear, (Miyauchi, 1984) as well as combined loading with shear and some other mode, such as tension (Barlat et al., 2003), with strains up to 0.5 attainable. With appropriately shaped specimens, the stress and strain distributions in the sample are relatively uniform for low strains. However, as the strains increase, shear bands may develop and end effects become

problematic (G'Sell et al., 1983). The strain levels at which this localization becomes a problem depends on both the material and geometry of the specimen.

These torsion and shear techniques, along with more exotic methods, such as thin-walled tubes under axial load and internal pressure (Hill et al., 1994), are valuable for understanding plastic behavior, especially at strains above the tensile uniform elongation; however, uniaxial, in-plane testing is often preferred for constitutive equation development because the deformation is uniform over the entire sampled volume and the results are more easily interpreted. Uniaxial compression testing of bulk material has been standardized in the industrial community (ASTM E9-89a, 2000) using cylindrical specimens with favorable aspect ratios to prevent buckling for strains over 0.05 (Arsenault and Pillai, 1996; Corbin et al., 1996; Yaguchi and Takahashi, 2005). Unfortunately, large-strain, in-plane compression is difficult to attain in sheet materials because of buckling modes that develop.

Compression testing of sheet material generally takes one of two forms. The first approach emulates the geometry of the bulk compression test, which has a length-to-diameter ratio of 3 (ASTM E9-89a, 2000). Following this approach, Bauschinger tests have been developed using small cylindrical (Bate and Wilson, 1986) or rectangular specimens (Abel and Ham, 1966; Karman et al., 2001). The effectiveness of these techniques depends on the particular gage-length/thickness ratio of the deforming sheet. Tests in the literature show attainable strain ranges that vary from 0.01 to 0.15 as the length/thickness ratio varies from 16 to 2 (Abel and Ham, 1966; Bate and Wilson, 1986). For comparison, a standard ASTM tensile bar requires a gage-length/thickness ratio greater than 2.67 and is often larger than 20 (ASTM E8-00, 2000). For higher-strain compression tests, where the length-to-thickness ratio approaches 2, the stress state in the deforming volume is unlikely to be either uniform or uniaxial. The other major disadvantages of this type of test are that the specimen size is often so small that the material may not be homogeneous for large-grained microstructures, and strain measurements using traditional methods can be difficult.

In-plane compression testing can also be accomplished using standard-sized specimens with side loading, or constraint, to suppress buckling in the thickness direction. Traditional techniques support the sides of the sample with a series of steel pins or rollers (Aitchison and Tuckerman, 1939; Ramberg and Miller, 1946), or use solid supports (Miller, 1944; Kotanchik et al., 1945; LaTour and Wolford, 1945; Moore and McDonald, 1945; Templin, 1945; Sandorff and Dillon, 1946; Zmievskii et al., 1972). A laminate of several samples may also be used in conjunction with side constraint in what has been called the "pack method" (Ramberg and Miller, 1946). These methods are unable to probe large strains because of buckling outside of the supported region. The largest unsupported length that can be tolerated for the above methods is approximately 1.25 mm, which typically enables compressive strains of 0.01–0.02 (Ramberg and Miller, 1946). In addition, samples cannot be continuously deformed during a tension/compression reversal because of the gripping arrangement. Studies of the Bauschinger effect using these methods require a two-step method where the sample is prestrained, unloaded, remounted, and then compressively loaded in another fixture. This is disadvantageous, particularly for cases where reverse flow begins before the sample is completely unloaded from the

initial tension. Continuous measurement is preferable for all reverse testing because it allows for consistent observation of the transition from tensile to compressive flow, and assures that little or no microstructural change or aging takes place during resting times between segments of the tests (Barlat et al., 2003).

Recent work utilizing solid supports has been reported by Tan et al. (1994) and Yoshida et al. (2002). Both groups used dogbone samples that could be pulled in tension and compression. To prevent buckling in the unsupported region, Tan et al. created small samples with gage-length-to-thickness ratios from 10 to 2, allowing compressive strains of 0.03 for the larger ratio and almost 0.20 for the smaller ratio. This hybrid approach, utilizing both small specimen size and side support, effectively improves the attainable strain range, but suffers from the same limitations of the small scale tests, in addition to buckling in the unsupported region. Yoshida et al. (2002) used a variation of the pack method, where 5 sheets were laminated together to provide support in addition to plates. This method was able to measure compressive strains up to 0.25 for mild steel and 0.13 for high strength steel.

Another approach to improve upon the limited strain range of supported specimens was developed by Kuwabara et al. (1995), who used two pairs of comb-shaped, or fork-shaped, dies to support the sample. This design is an improvement over the solid supports because, as the sample is compressed, the male and female dies slide past each other allowing the entire length of the specimen to be supported. By eliminating the interference problem between the platens and the support fixture, strains on the order of 0.15–0.20 were attainable for single sheets of material under compressive loading (Kuwabara et al., 1995). Balakrishnan and Wagoner (1999) extended this method to test unlaminated sheet material in continuous, sequential, compression/tension tests. Special fixtures were designed for use with a standard tensile frame and a dogbone specimen. The sample was sandwiched between two sets of fork-shaped supports, similar to those of Kuwabara et al. (1995) and a supporting force was applied to the sample using a hydraulic hand pump. This device was able to achieve compressive strains of 0.08 continuously during both reversed and cyclic tests (Balakrishnan, 1999; Geng and Wagoner, 2002).

The fork devices have several limitations. The specimen design is rather long and slender, and it is difficult to maintain axial alignment of the tensile axis for various sheet thicknesses. This misalignment leads to reductions in the compressive strain range attainable before buckling. The misalignment can be compensated for, to some extent, by increasing the side load, but this introduces increased error through larger friction and stress biaxiality. From a practical standpoint, repeated use at the required large force eventually damages the forks, which are expensive and complex to machine for periodic replacement.

In the current work, a new test design was sought combining the advantages of the miniature, side-supported tests – continuous, large-strain, reversed strain paths – with the practical advantages of larger specimen sizes – homogeneity, self-alignment in a standard tensile testing machine, and simple, accurate measurement of uniform stress and strain.

2. New tension/compression approach

In order to avoid the limitations of existing designs for in-plane compression, a new approach was developed, shown in Fig. 1. Solid, flat plates are used for buckling constraint, and a special specimen design was developed to minimize buckling outside of the constrained region. The solid plates offer several advantages over fork designs including better self-alignment, much easier machining, and better durability. As will be shown, the improved alignment also allows reduced constraining force, and therefore more-nearly uniaxial loading.

Replacing the forks with solid side plates reintroduces an undesirable (for buckling) unsupported region of the specimen. To prevent the sample from buckling in this region, an exaggerated dogbone specimen was designed to assure the load in the unsupported gap will be lower than the critical buckling load. By adjusting the dimensions of the sample, a large enough clearance can be sustained to allow considerable stable compressive strain.

The clamping system used to provide side support for the fork device (Balakrishnan, 1999) was modified slightly for the new method, Fig. 2. The same Enerpac™ P141 hand pump and RWH200 hydraulic cylinder are used to apply a restraining force to the sample through four sets of hardened steel rollers. In the previous fork device, this assembly was bolted into the fixture that held the sample. Because this fixture was eliminated for the new method, the clamping assembly currently attaches to the bottom hydraulic grip. The entire assembly is mounted on an Instron™ 1322 test frame and operated using an Interlaken™ 3200 series controller. The hydraulic clamping system is a significant improvement over the other methods discussed earlier. Control of the supporting force at a specific value allows for more robust biaxial and friction corrections than in systems where the support is provided by plates

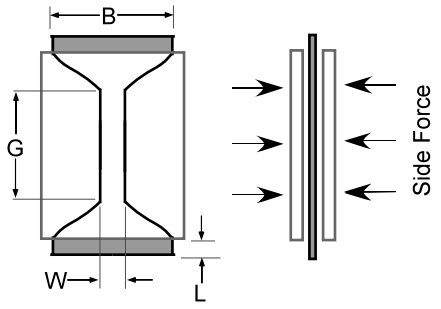

Fig. 1. Schematic of the flat plate supports and final sample dimensions.

Fig. 2. Assembly of new plate method.

connected by bolts or springs, where the actual supporting force is unknown or uncontrolled.

The experimental conditions were optimized to achieve two competing goals: maximize the attainable compressive strains, and maximize the uniformity of strain and stress in the gage length of the specimen. Buckling and strain distribution analysis were conducted using commercial finite-element analysis software (ABAQUS Inc., 2003). Two models were used. One was an explicit analysis using 600 linear solid elements to probe the buckling behavior. The other analysis modeled one-quarter of the sample using an implicit model containing 7260 quadratic elements to observe the stress and strain distribution.

When optimizing the part, there are essentially three buckling failure modes that need to be suppressed: buckling in the thickness direction within the supports (t-buckling), buckling in the unsupported gap (L-buckling), and buckling in the width direction (W-buckling). If these three modes are suppressed, the measurable strain is eventually limited by the non-uniformity introduced by barreling in the gage region. Examples of these four failure modes are shown in Fig. 3.

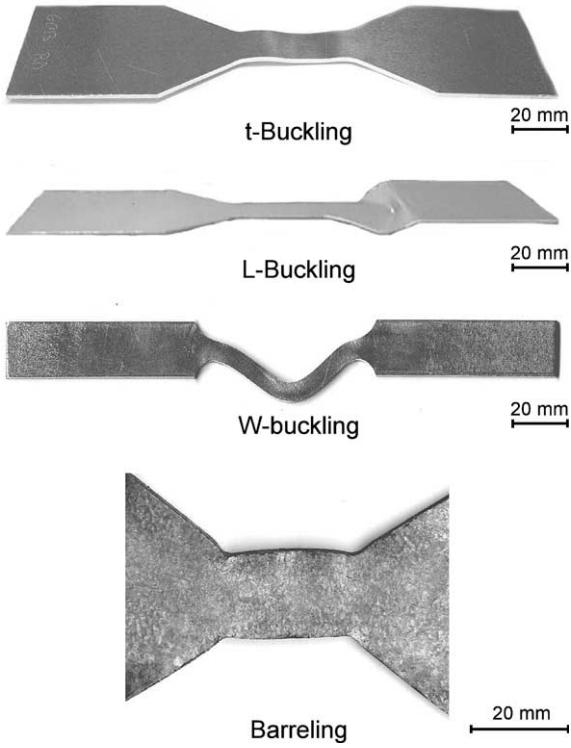

Fig. 3. Examples of specimen failure though *t*-buckling, *L*-buckling, *W*-buckling and barreling.

2.1. Optimization of sample geometry

Regions of the sample that are prone to buckling can be optimized using standard column buckling equations. The eccentricity of a load applied to a column creates a bending moment, which must be supported in addition to the axial force. The secant formula, found in many mechanics books, (Beer and Johnston, 1993; Hibbeler, 1997) calculates the maximum stress, $\sigma_{\max}$, in a column from the combined effects of the axial force and bending moment:

$$\sigma_{\max} = \frac{P}{A}\left[1 + \frac{ec}{r^2}\sec\left(\frac{L_e}{2r}\sqrt{\frac{P}{EA}}\right)\right], \tag{1}$$

where,

P	axial load
A	cross sectional area of the column
e	eccentricity of the load, as measured from the column neutral axis to the line of action of the force
c	distance from the neutral axis to the outer fiber where $\sigma_{\max}$ occurs
L_e	effective length of the column in bending plane = $L/2$ for fixed ends

E elastic modulus
r radius of gyration, $r^2 = I/A$, where I is the moment of inertia computed about the bending axis.

The maximum stress approaches infinity as the value within the secant approaches $\pi/2$; this point marking the stability limit for the column. It is equivalent to the value of the critical buckling load determined by the Euler method (Beer and Johnston, 1993; Hibbeler, 1997),

$$P = \frac{\pi^2 EI}{L_e^2}. \tag{2}$$

Another feature of Eq. (1) is that for short, squat columns, the value of the secant approaches one and Eq. (1) reduces to,

$$\sigma_{\max} = \frac{P}{A}\left[1 + \frac{ec}{r^2}\right], \tag{3}$$

which can be rearranged in terms of load as follows:

$$P = \frac{A\sigma_{\max}}{\left[1 + \frac{ec}{r^2}\right]}. \tag{4}$$

For these short columns, (such as the unsupported gap region of the tension/compression specimen) failure is caused by plastic yielding of the column rather than buckling. The eccentricity of the load only serves to increase the stress by the moment it induces. When Eq. (4) is used for design, $\sigma_{\max}$ is often set to the yield stress, predicting the maximum elastic load the column can sustain. This is a conservative criterion because the onset of buckling may not coincide with the start of plastic deformation. Substituting the sample dimensions, introduced in Fig. 1, Eq. (4) becomes

$$P = \frac{Bt\sigma_y}{\left[1 + \frac{6e}{t}\right]}. \tag{5}$$

In terms of the specimen geometry, the flow stress in the gage region is $\sigma_f = P/Wt$. Solving this relation for P and substituting into Eq. (5), predicts the maximum flow stress that can be tested before plastic deformation initiates in the unsupported gap as a function of the sample design and specimen thickness,

$$\sigma_f^{\text{max before } L\text{-buckling}} = \frac{B\sigma_y}{W\left[1 + \frac{6e}{t}\right]}. \tag{6}$$

If the function $\sigma_f = f(\varepsilon)$ and its inverse $\varepsilon = f^{-1}(\sigma_f)$ are known, then Eq. (6) can alternatively be framed in terms of a maximum strain criterion.

Because W-buckling occurs in the gage region, where yielding is necessary, an alternate method must be used to establish the limit strain. The question becomes not whether the column is yielding, but whether this deformation is stable. This is the same question asked in the Euler method, which led to Eq. (2). Because the gage

region is plastically deforming during the test, the elastic modulus must be replaced with the tangent modulus and Eq. (2) becomes

$$P = \frac{\pi^2 E_t I}{L_e^2}, \tag{7}$$

where E_t is the tangent modulus, $d\sigma_f/d\varepsilon$ evaluated at P. Again, substituting the test geometry and the relationship between P and the flow stress gives,

$$\sigma_f^{\text{max before } W\text{-buckling}} = \frac{\pi^2 E_t W^2}{3G^2}. \tag{8}$$

Note this equation is only a function of the gage width and length, and unlike Eq. (6), is independent of the sample thickness. Eqs. (6) and (8), in conjunction with knowledge of a material's stress–strain relationship, enable the calculation of the maximum compressive strain attainable for any sample geometry before L or W-buckling.

Because the sample optimization depends on the mechanical properties of the specimen, the optimal sample geometry differs with the material. The material used in the initial optimization of the specimen geometry was aluminum alloy 6022-T4 from the same lot used by Balakrishnan and Wagoner (1999) which has a thickness of 2.5 mm. The effect of material on the optimization results will be shown by comparing 6022 to aluminum-killed-drawing-quality (AKDQ) steel and Mg alloy AZ31B of the same thickness. The elastic modulus and assumed flow curves for these three materials are as follows:

$$\begin{aligned}
&6022: \quad E = 69 \text{ GPa}, \quad \sigma = 389 - 220e^{-8.44\varepsilon} \quad \text{(Balakrishnan, 1999)},\\
&\text{AKDQ:} \quad E = 202 \text{ GPa}, \quad \sigma = 522\varepsilon^{0.22} \quad \text{(Unpublished Research)},\\
&\text{AZ31B:} \quad E = 45 \text{ GPa}, \quad \sigma = 323 - 172e^{-13.05\varepsilon} \quad \text{(Unpublished Research)}.
\end{aligned} \tag{9}$$

These relations are fit to a strain range starting from the 0.002 offset yield point and extending to a strain of 0.10 for AKDQ, 0.19 for magnesium, and 0.27 for 6022.

Using the relationships introduced above, the sample geometry can be optimized following the procedure summarized in Fig. 4. Each of the variables in Eqs. (6) and (8) affects the attainable compressive strain range, but there are external constraints on these values. For example, the width of the grip region, B, should be as large as possible to discourage buckling in the unsupported region, but the size of the hydraulic grips available for the current work, 50 mm, limits this dimension. Buckling outside the gage is progressively inhibited for smaller gaps, L; but L mechanically limits the compressive strain that can be attained. Also, Eq. (8) shows that reducing G suppresses in-plane buckling tendencies. However, as mentioned in previous discussions, G must remain large enough so that the stress state in the measured gage length is uniform and uniaxial. A trial G, chosen at the beginning of the process, must be checked at the end of the optimization procedure to assure this condition is satisfied.

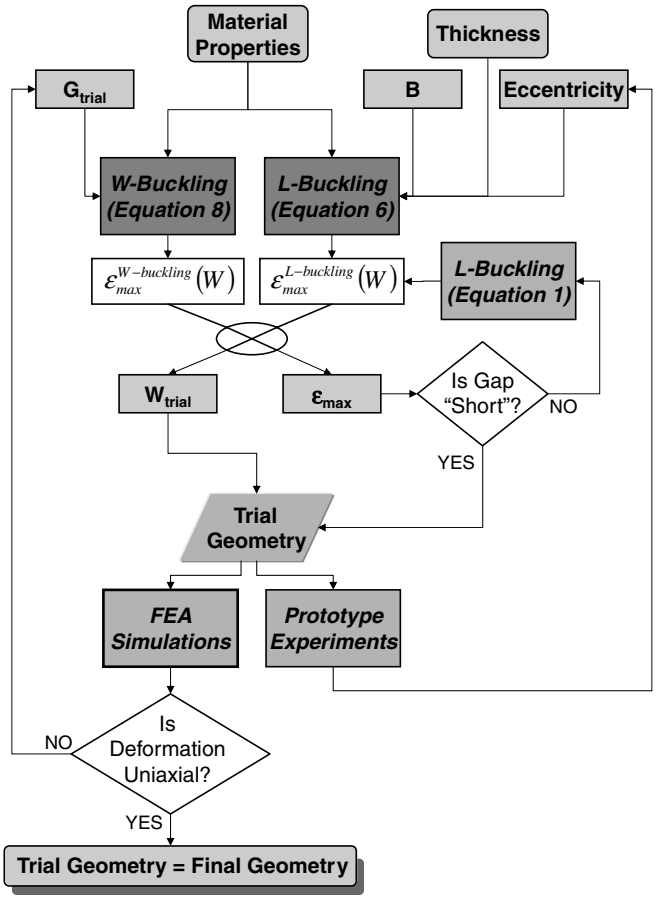

Fig. 4. Procedure for optimizing sample geometry though FEA simulations and experiments.

Once a material and trial gage length are chosen, Eq. (8) can determine the maximum flow stress before W-buckling as a function of the gage width, W. Using the material flow law, this result can be presented in terms of the maximum attainable compressive strain before W-buckling, $\varepsilon_{\max}^{W\text{-buckling}}$. Fig. 5 shows this relationship for 6022, AKDQ steel and Mg-AZ31B for a gage length of 36.8 mm. This figure indicates that the maximum attainable compressive strain is sensitive to the flow curve of the material, and is only reliable in the range where the flow stress equation is known accurately. The deviation of the steel curve from the other two materials at large widths is because the equations describing strain hardening of Mg and Al are of the saturation type (Voce, 1948), while hardening for steel is better described by a power-law equation (Hollomon, 1945).

In a similar manner, Eq. (6) can predict the dependence of W on the maximum strain before L-buckling, $\varepsilon_{\max}^{L\text{-buckling}}$. The inputs for this prediction are the flow

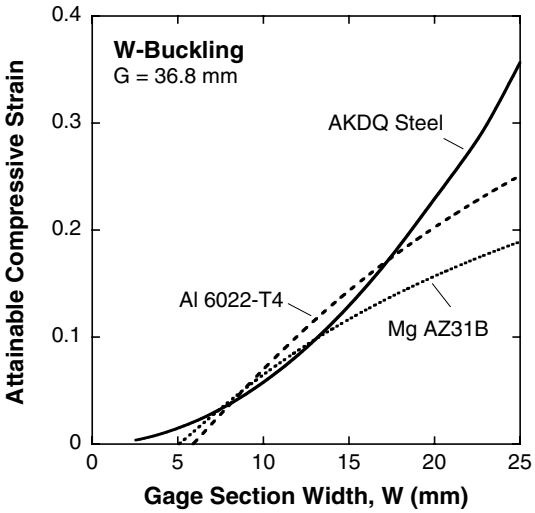

Fig. 5. Maximum compressive strain attainable as a function of sample width before *W*-buckling.

equations, the value of B, sheet thickness, and an estimate of the load eccentricity, which must be determined experimentally for a given machine and fixture. Fig. 6 shows the maximum attainable strain before buckling as a function of width for 6022. The intersection of these two curves indicates the optimum gage width for this particular material and thickness. For each thickness, the intersection of the *L* and *W*-buckling curves gives a width, which is plotted as a function of thickness in Fig. 7. This curve represents the optimum width and thickness combination. Samples with

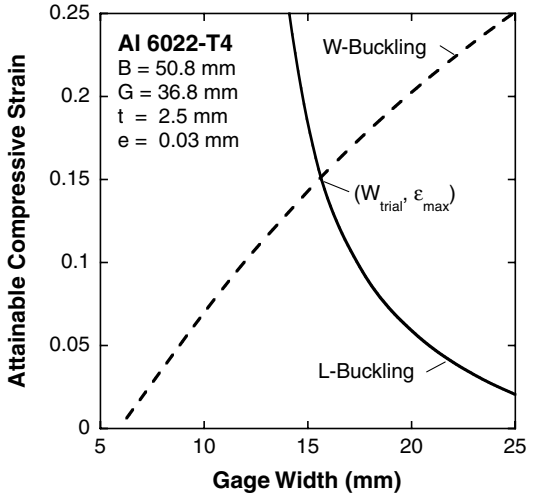

Fig. 6. Maximum compressive strain attainable as a function of sample width for *L*- and *W*-buckling.

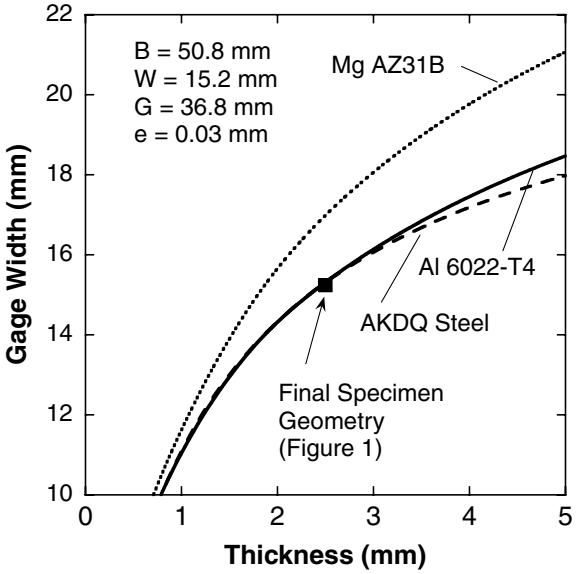

Fig. 7. Optimum relationship between sample width and thickness.

dimensions lying to the left of this curve are too thin and will buckle in the gap at a strain lower than the maximum strain that was predicted in Fig. 6. Samples that lie to the right are thick enough to resist L-buckling, and will not benefit from increased thickness because of the independence of thickness on W-buckling, shown in Eq. (8). The final sample dimensions used in this work are shown by the square in Fig. 7, and were listed in Fig. 1. One can note that although this geometry was derived for 6022, it is nearly optimal for AKDQ, but is not optimized for Mg AZ31B.

Fig. 6 also indicates the maximum compressive strain that the specimen can attain, which determines the necessary gap, L, to prevent mechanical interference between the supports and the grips. The minimum possible L is 3 mm, which is the smallest gap that can be consistently attained with the current fixture. After the size of the gap is determined, it is possible to evaluate whether or not the short column assumption, which led to Eq. (6), is valid for the trial geometry. If Eq. (6) is not valid, Eq. (1) must be solved iteratively instead. For the case in Fig. 6, where the suggested L is 5.5 mm, the short column assumption results in a specimen width within 0.05% of the answer obtained using Eq. (1). For a gap of 10 mm, the error associated with the assumption increases to 0.2% and for a gap of 20 mm the two methods only differ by 1.05%, suggesting that for most cases the short column assumption is very robust.

Once the trial geometry is created, it can be tested experimentally and these results can be fed back into the analysis to refine the value of the eccentricity. To determine the eccentricity, a design should be chosen that is prone to L-buckling, such as one with a small thickness or large W. In this case, 6022 with a thickness of 0.9 mm was available. In repeated tests of this material, the maximum strain attainable before

L-buckling was 0.01. The buckling map for this thinner material was created and the value of the eccentricity was adjusted until the curve describing the L-buckling had a maximum strain of 0.01 at a width of 15.2 mm. As seen in Fig. 8, this corresponds to an eccentricity of 0.3 mm.

After the trial geometry is determined, finite-element simulation is used to find a gage length that provides a uniform, uniaxial stress state over the entire measurement range of a 25.4 mm extensometer. In a finite-element model, each design and the ASTM tensile standard are loaded to the same stress. The strain is calculated using a "virtual extensometer" by measuring the relative displacement of two material points initially 25.4 mm apart. The gage length, G, is adjusted until the strain measured from the new geometry agrees with the results from the ASTM sample within a desired tolerance. Some iteration is required to find this value as the other dimensions of the sample will change. The final gage length chosen for 6022 was 36.8 mm, which differed from the ASTM standard by 1.2% after 0.075 strain.

2.2. Optimization of the supporting force

The clamping force of the supporting plates also affects the failure mode. If the clamping force is too large, frictional effects redistribute the load from the gage region onto the material that is in the unsupported gap, leading to L-buckling at the entrance of the fixture. However, if the clamping force is too small, the plates will not prevent wrinkling, or t-buckling. Using the ABAQUS/Explicit buckling model, these two extreme failure modes can be observed, with t-buckling at low side force and L-buckling at higher forces. In between these two extremes, there is a peak in the compressive strain obtained before failure, seen in Fig. 9. The optimum side force is about 7 kN, where the side forces are sufficient to prevent t-buckling, yet the

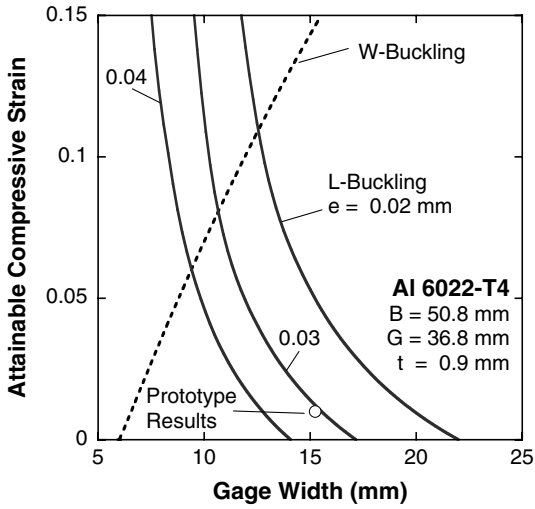

Fig. 8. Determination of load eccentricity by matching results from prototype specimens.

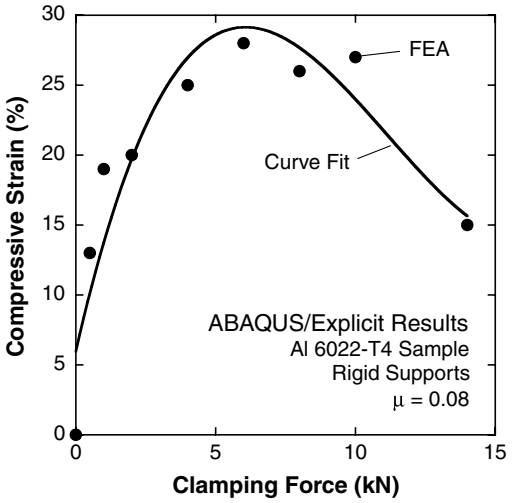

Fig. 9. Results of maximum attainable compressive force before failure, as a function of clamping force, calculated from FEM experiments.

frictional effects are minimized. This is considerably lower than the forces used in the fork device, which were 12.5 kN for 6022 and up to 19 kN for HSLA steel (Balakrishnan, 1999). In practice, the range from 5 to 10 kN has proven to be acceptable, although higher forces are sometimes needed for thinner material, or when testing to high compressive strains, where the flow stress becomes large.

2.3. Strain measurement

Because the flat side plates are in contact with the entire surface of the sample, it is impossible to attach strain gages or mount an extensometer in the conventional way. During the initial phase of the optimization program, a mechanical extensometer was mounted on the edge of the specimen. To assure the supporting plates did not come into contact with the extensometer blades, it was necessary to position the plates so as to create a small unsupported ledge on which to mount the extensometer. This free edge caused significant wrinkling and buckling of this side of the sample face. Current tests (including the results shown later in Fig. 13) use a non-contact, EIR™ laser extensometer, which enables the plates to cover the entire surface of the specimen. Initial results show this is an effective way to eliminate buckling along the edge.

2.4. Uniaxial data corrections

Because of the need to constrain the sample in the thickness direction to prevent buckling, all raw stress–strain results require corrections for frictional and biaxial effects arising from this supporting force. The addition of a constraining force, F_2

creates a readily calculated through-thickness stress, σ_2. Knowing this value, the Von Mises effective stress is

$$\bar{\sigma} = \sqrt{\frac{1}{2}\left[(\sigma - \sigma_2)^2 + \sigma_2^2 + \sigma^2\right]}, \tag{10}$$

where σ is the axial testing stress. Because the thickness stress is much smaller than the stress in the testing direction, the biaxial effect is small and the choice of the constitutive equation defining the effective stress is not critical. If Eq. (10) is replaced with an effective stress based on Hill's anisotropic yield surface with $r = 0.6$, (Hill, 1948) the two curves differ by 0.4%.

The friction correction is more significant and more complex because the direction of the frictional force reverses when the loading direction changes. To reduce friction, the side supports are covered with a 0.35 mm Teflon sheet, and the supporting force is transmitted from the hydraulic pump to the supports through a series of rollers that allow the plates to move with the sample along the loading axis.

The actual force deforming the sample, F_{deform}, is the value measured from the load cell, F_{meas}, with the additional frictional force, F_{friction} subtracted,

$$F_{\text{deform}} = F_{\text{meas}} - F_{\text{friction}}. \tag{11}$$

The frictional behavior is represented by a Coulomb friction law (Wagoner and Chenot, 1996) as follows:

$$F_{\text{friction}} = \mu F_2, \tag{12}$$

where μ is the friction coefficient, which is assumed to be the same in tension and compression. When the load is reversed, there is a range equal to $2F_{\text{friction}}$, where the external load, applied by the tensile frame, is changing to overcome friction in the new direction; however, the internal load on the sample is constant. The data points measured within this range are not included in the corrected results.

The magnitude of the frictional effect has been estimated by Balakrishnan (1999), who found a friction coefficient in the range of 0.06–0.09 by measuring changes in the yielding force of nominally identical samples as a function of side force. This range corresponds to a difference in the flow stress of about 4% for a 5 kN side force. Although this method gives satisfactory results, it can be complicated by material, contact, and geometry variation requiring several tests to gage variability. Some variability in the friction coefficient is expected, related to variations in the sample surface condition and accumulated damage to the Teflon coating. Therefore in practice, the friction coefficient is adjusted slightly so that the supported, tensile deformation matches the baseline, unsupported curve. When the friction coefficient is adjusted in this way, the values used are never larger than the range 0.06–0.09 predicted by Balakrishnan with the fork device. In fact for the new plate method, values around 0.03–0.06 produce better agreement between the supported and unsupported flow curves. Fig. 10 shows the relative effects of each step in the data corrections. After both friction and biaxial corrections, the flow curve of the supported sample agrees well with the unsupported uniaxial tension test with a standard deviation between the two curves of under 0.1 MPa.

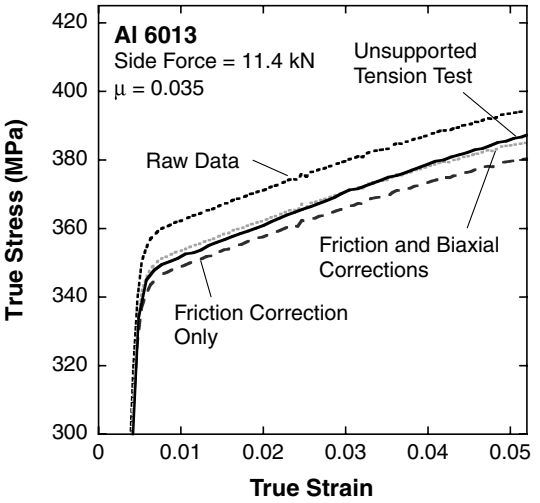

Fig. 10. Comparison of data after friction and biaxial corrections to an unsupported tensile test.

2.5. Experimental validation of method

The results of reverse loading experiments on AA-6022 obtained with the new approach are consistent with those obtained using the older, established, fork device, Fig. 11. It is apparent both approaches reveal the same features of the Bauschinger effect, however, tests using the flat plate supports show much smoother stress–strain

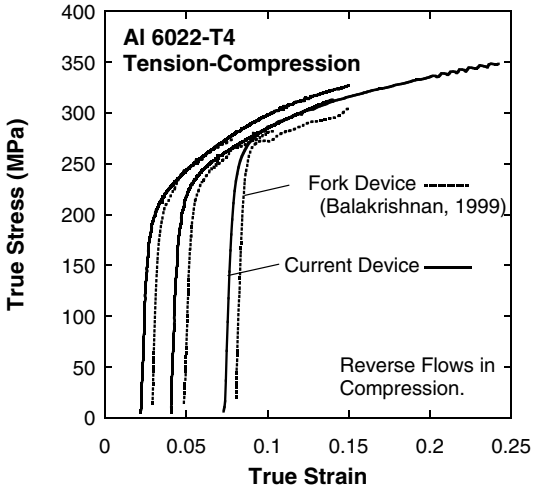

Fig. 11. Comparison of current flat-plate device to previously used fork device for compression after tensile prestrain.

behavior in compression, and larger attainable strains. Fig. 12 shows reloading curves for tension/compression and compression/tension tests using the new device. The results are nearly symmetric with respect to tension and compression, suggesting the new method successfully stabilizes the compressive loading and leads to compressive stress–strain curves that are comparable with uniaxial tension.

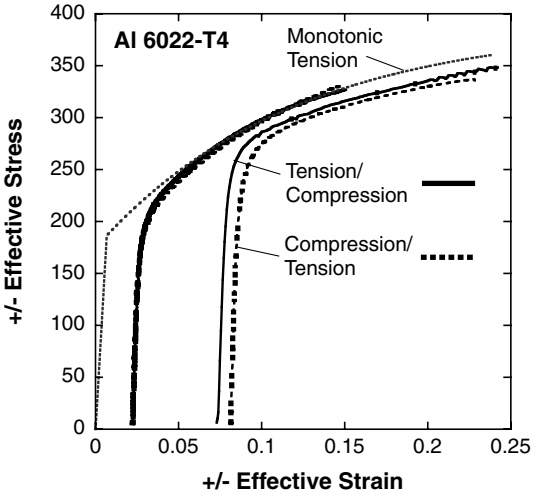

Fig. 12. Comparison of tension/compression and compression/tension curves for the new method.

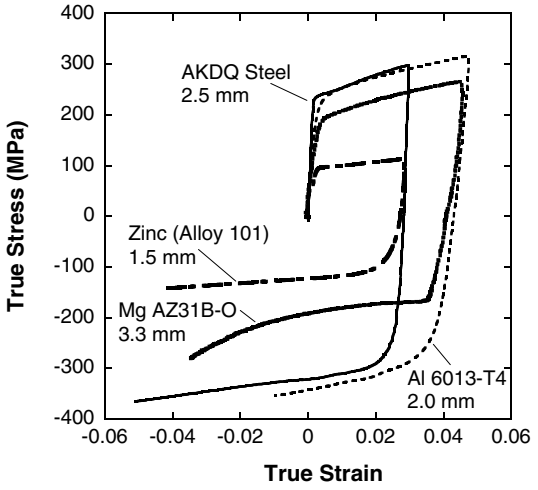

Fig. 13. Tension/compression test for Al, Mg, Zn and AKDQ steel.

3. Demonstration of capabilites of the new method

3.1. Testing of the Bauschinger effect and material hardening

Since the new measurement method was established, it has been used to study the Bauschinger effect. The flat plate supports were successful in allowing continuous measurement of reverse loading in both tension and compression under displacement control for a variety of prestrains and materials. Several different aluminum, magnesium, zinc and steel samples with various thicknesses greater than 1 mm have been tested, Fig. 13. The robustness of the method can be seen in the attainable strain range and the smoothness of the stress–strain curves. (The asymmetric behavior of Mg in tension and compression is physical in nature, caused by twinning.)

Tests to determine the effect of heat treatment and sheet texture on the Bauschinger effect have been performed on two aluminum alloys 6013 and 2524, with sheet thicknesses of 1.98 and 1.75 mm, respectively. Representative curves from 2524 and 6013 for various heat treatments are shown in Fig. 14 and 15. For 6013, heat treatment alters the relative flow stress and hardening rates of the materials, but does not drastically change the form of the Bauschinger behavior. All three conditions show similar yield point reductions and hardening transients. Alloy 2524, on the other hand, shows very different behavior in the artificially aged condition than in the other tempers. In the presence of incoherent precipitates, the artificially aged sample has a severely reduced yield point and an inflection in the reloading curve. This same inflection has been observed for 2024, which has a similar alloy content to 2524 (Stoltz and Pelloux, 1976; Hidayetoglu et al., 1985). Fig. 16 shows the reloading curves of several artificially aged 2524 samples for two prestrains and three

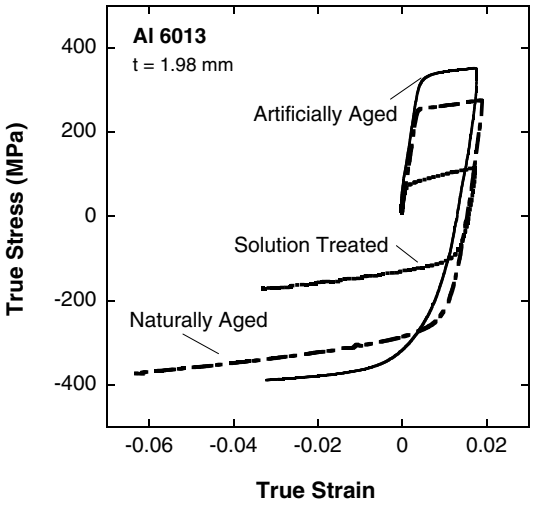

Fig. 14. Reverse loading curves of AA-6013 for various tempers.

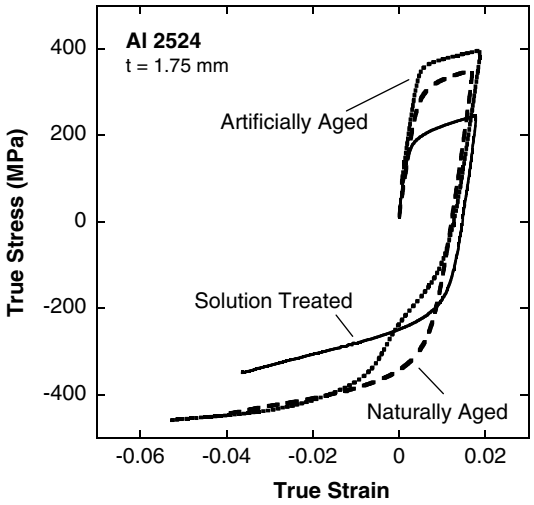

Fig. 15. Reverse loading curves of AA-2524 for various tempers.

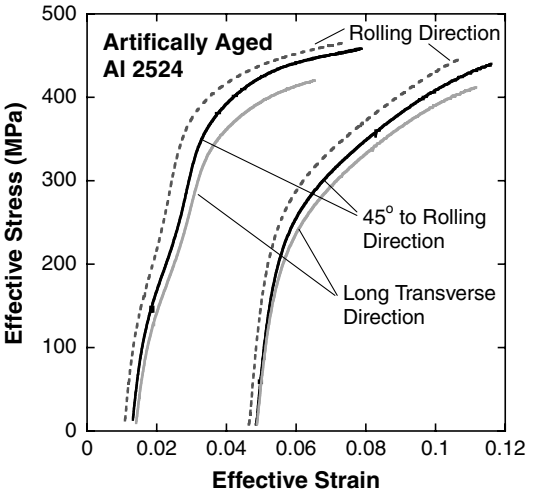

Fig. 16. Reverse loading curves of artificially aged AA-2524 in three sheet orientations and two different prestrains.

different test orientations (rolling direction, transverse direction, and 45° to the rolling direction). The difference in the flow curves of each orientation is because of the planar anisotropy of the sheet. The inflection of the reloading curve is observed in all three sheet orientations, but only at small prestrains.

3.2. Cyclic hardening and ratcheting tests

Being able to measure continuous tension and compression for samples of different conditions and texture orientations, allows for many other tests that can be used for constitutive equation development. Cyclic hardening tests under strain control, Fig. 17, and ratcheting tests under load control, Fig. 18, were demonstrated using high-strength, low-alloy steel (HSLA-50) with a thickness of 1.63 mm (Ghosh and

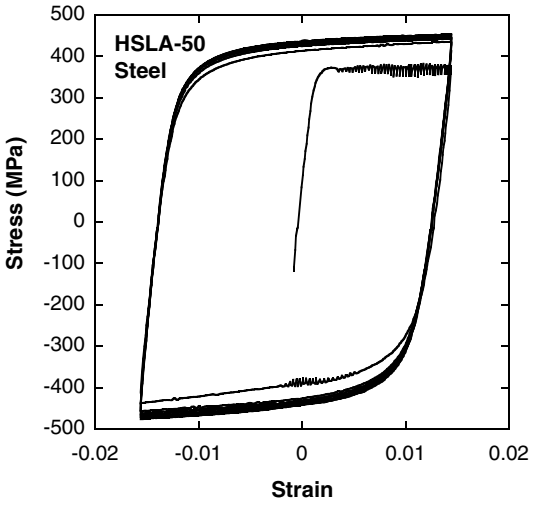

Fig. 17. Cyclic hardening curve for HSLA-50 steel for 8 cycles.

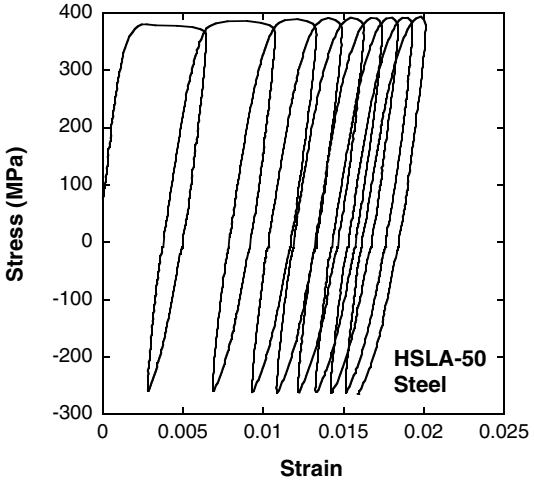

Fig. 18. Ratcheting results for HSLA-50 steel.

Xie, 2004). Much of the previous research on cyclic hardening and ratcheting uses cylindrical samples, (Stoltz and Pelloux, 1976; Hidayetoglu et al., 1985; Plumtree and Abdel-Raouf, 2001) which has different properties than rolled sheet. Only recently has information from sheet material been used, such as Kang et al. (2003) using data from Yoshida et al. (2002). The ability to conduct these tests on textured sheets with a relatively simple device gives valuable baseline information on saturation behavior that is essential to development of robust material models for sheet material.

3.3. Room temperature creep after load reversal

The anelastic contribution to creep has been carefully examined through the use of stress-dip tests by researchers, including Gibeling and Nix (1981). In the stress-dip test, the load is quickly reduced while the strain transient is measured. This new technique has the ability to extend this method by allowing the stress to be completely reversed. This procedure has been used to measure the effects of room-temperature creep of aluminum alloy 6022 after reverse loading.

The Instron™ tensile frame was used in load control while the strain was recorded using a National Instruments™ NI-4350 voltage measurement device capable of measuring smaller strain changes. The samples were loaded to an initial value of $\sigma_0 = -240$ MPa at 8 MPa/s. This load roughly corresponds to a compressive strain of 0.07. After reaching this load level, the load was changed at the same rate to a new value ranging from 75% of the original flow stress and held for 1 h. Fig. 19 shows results from a series of such tests, showing the creep rates for various degrees of load reversal. Note that because the initial loading (σ_0) is compressive, the curves labeled $-0.75\sigma_0$, $-0.50\sigma_0$ and $-0.25\sigma_0$ correspond to tensile loading. At stresses near the

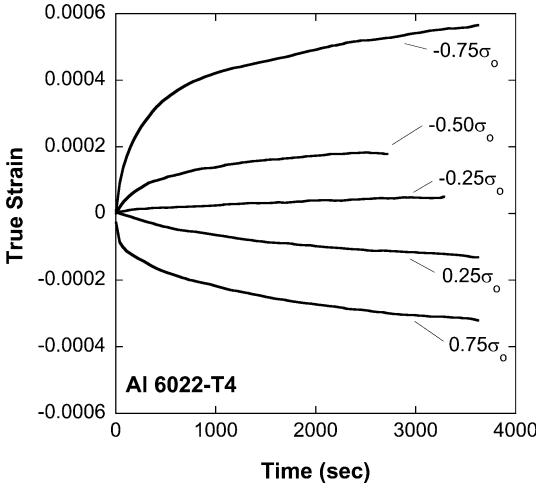

Fig. 19. Room temperature creep results from AA-6022.

flow stress, the creep rate in the same direction as the initial loading is slower than the rate for the same load in the reversed direction. A more refined series of tests similar to these could be used to ascertain the backstress in the material, induced by the prestrain as the stress value where the strain rate is zero. Similar techniques that probe a variety of different prestrains and/or loading rates could also be used to develop a strain-dependent room-temperature creep laws for materials that experience a load reversal. One factor that must be assessed when performing these creep tests is to assure the side force does not adversely affect the creep results because the strains are so small. For a stress reversal, the problem can be avoided entirely by making the initial deformation in the compressive direction, then releasing the side force for the reversed tensile creeping. In this way, the results are completely free from any frictional or biaxial effects.

3.4. Anelasticity after strain reversal

Like creep, anelasticity is another time-dependent effect that is altered by reverse deformation. Specimens of Al-6022 and drawing-quality-silicon-killed (DQSK) steel were first compressively loaded to a true strain of −0.045 using the plate supports. The samples were then unloaded and the clamping device was removed so an extensometer could be securely attached to the wide portion of the specimen to assure the most accurate strain measurement. An additional tensile strain, $\varepsilon_{ten,}$ was applied to the samples, after which, the load was quickly dropped to zero by opening the hydraulic grips. Removing the instantaneous elastic contraction, Fig. 20 shows the anelastic strain change at zero applied stress with time for both 6022 and DQSK steel. For large strains after the reversal, ($\varepsilon_{ten} = 0.11$) the sample behaves similarly to a uniaxial test. That is, after the grips are opened and the sample is unloaded, there is some anelastic response that contracts the sample, producing a negative

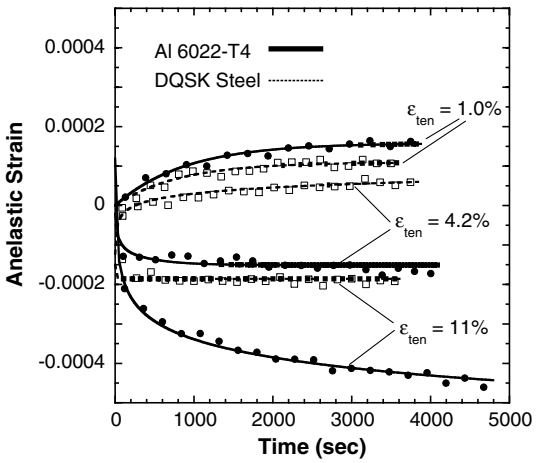

Fig. 20. Results from anelastic testing of AA-6022 and DQSK steel.

strain that accumulates with time. For smaller reversals, the behavior is quite different, and perhaps somewhat surprising. After the tensile load is removed, the sample again shows an anelastic response, although in the opposite direction. The elongation of the sample with time is likely attributable to the structure and dislocation arrangement from the initial compressive loading that persists during the initial stages of reversed tensile loading. The same mechanisms appear to be present in both steel and aluminum alloys as seen from the similarities in the curves for each material. Wang and Wagoner (Wang et al., 2004) have used these results to assess the possible influences of this sort of anelasticity on the time-dependent springback of aluminum alloys and concluded that it may have some effect during the first few minutes after removal from the die.

4. Conclusions

(1) A new method has been developed for measuring continuous tension/compression curves of sheet metal using a tensile frame and some simple tooling. The criteria for specimen optimization were established, and curves and techniques for estimating the limits of the measurable strain as a function of sample material and geometry were presented.
(2) The ability to control hydraulically a known supporting force gives this new method distinct advantages over other in-plane compression techniques by enabling optimization of the side force, and providing input to more robust corrections for frictional and biaxial effects.
(3) Compared to the previous fork method, the new design and optimization procedure doubles the attainable strain range and produces much smoother compressive flow. This improvement is accomplished while significantly decreasing the necessary side force, leading to reduced frictional and biaxial effects.
(4) The new device also allows for efficient exploration of many different types of physical phenomena associated with non-proportional loading of sheet metals, including room-temperature creep, and anelasticity.

Acknowledgments

Special thanks to the Alcoa Technical Center, Alcoa Center, PA, for providing the aluminum alloys used in this work to the Ohio Supercomputer Center under contract PAS 080, and to the National Science Foundation for their financial support under award number DMR-0139 45.

References

ABAQUS Inc., 2003. Explicit Dynamic Analysis. ABAQUS Version 6.4 Documentation: ABAQUS Analysis User's Manual. Pawtucket, RI, ABAQUS, Inc.

Abel, A., 1987. Historical perspectives and some of the main features of the Bauschinger effect. Mater. Forum 10 (1), 11–26.

Abel, A., Ham, R.K., 1966. The cyclic strain behavior of crystals of aluminum-4 weight percent copper: I. Bauschinger effect. Acta Metall. 14 (11), 1489–1494.

Aitchison, C.S., Tuckerman, L.B., 1939. The Pack Method for Compressive Tests of Thin Specimens of Materials Used in Thin-wall Structures. National Advisory Committee on Aeronautics, Washington, DC, T.N. No. 649.

Anand, L., Kalidindi, S.R., 1994. The process of shear band formation in plane strain compression of fcc metals: effects of crystallographic texture. Mech. Mater. 17, 223–243.

Arsenault, R.J., Pillai, U.T.S., 1996. The Bauschinger effect in a SiC/Al composite. Metall. Mater. Trans. A 27 (4), 995–1001.

ASTM E8-00, 2000. Standard Test Methods for Tension Testing of Metallic Materials. ASTM, West Conshohocken, PA.

ASTM E9-89a, 2000. Standard Test Methods for Compression Testing of Metallic Materials at Room Temperature. ASTM, West Conshohocken, PA.

Balakrishnan, V., 1999. Measurement of in-plane Bauschinger effect in metal sheet. MS Thesis. The Ohio State University, Columbus, OH.

Barlat, F., Duarte, J.M.F., Gracio, J.J., Lopes, A.B., Rauch, E.F., 2003. Plastic flow for non-monotonic loading conditions of an aluminum alloy sheet sample. Int. J. Plasticity 19 (8), 1215–1244.

Bate, P.S., Wilson, D.V., 1986. Analysis of the Bauschinger effect. Acta Metall. 34 (6), 1097–1105.

Bauschinger, J., 1886. On the change of the elastic limit and the strength of iron and steel, by drawing out, by heating and cooling, and by repetition of loading (summary). In: Minutes of Proceedings of the Institution of Civil Engineers with Other Selected and Abstracted Papers LXXXVII: 463.

Beer, F.P., Johnston, E.R., 1993. Mechanics of Materials. McGraw Hill, New York.

Brown, G.M., 1970. Inelastic deformation of an aluminum alloy under combined stress at elevated temperature. J. Mech. Phys. Solids 18 (6), 383–396.

Chaboche, J.L., 1989. Constitutive equations for cyclic plasticity and cyclic viscoplasticity. Int. J. Plasticity 5 (3), 247–302.

Chen, Z., Maekawa, S., Takeda, T., 1999. Bauschinger effect and multiaxial yield behavior of stress-reversed mild steel. Metall. Mater. Trans. A 30 (12), 3069–3078.

Chun, B.K., Jinn, J.T., Lee, J.K., 2002. Modeling the Bauschinger effect for sheet metals, part I: theory. Int. J. Plasticity 18 (5–6), 571–595.

Colak, O.U., 2004. A viscoplastic theory applied to proportional and non-proportional cyclic loading at small strains. Int. J. Plasticity 20 (8–9), 1387–1401.

Corbin, S.F., Wilkinson, D.S., Embury, J.D., 1996. The Bauschinger effect in a particulate reinforced Al alloy. Mater. Sci. Eng. A 207 (1), 1–11.

Geng, L., 2000. Application of plastic anisotropy and non-isotropic hardening to springback prediction. PhD Thesis. The Ohio State University, Columbus, OH.

Geng, L., Shen, Y., Wagoner, R.H., 2002. Anisotropic hardening equations derived from reverse-bend testing. Int. J. Plasticity 18 (5–6), 743–767.

Geng, L., Wagoner, R.H., 2002. Role of plastic anisotropy and its evolution on springback. Int. J. Mech. Sci. 44 (1), 123–148.

Ghosh, S., Xie, C., 2004. In: Ghosh, S. et al. (Eds.), Modeling Cyclic Deformation of HSLA Steels Using Crystal Plasticity. American Institute of Physics, Melville, NY.

Gibeling, J.C., Nix, W.D., 1981. Observations of anelastic backflow following stress reductions during creep of pure metals. Acta Metall. 29 (10), 1769–1784.

G'Sell, C., Boni, S., Shrivastava, S., 1983. Application of the plane simple shear test for determination of the plastic behavior of solid polymers at large strains. J. Mater. Sci. 18, 903–918.

Hibbeler, R.C., 1997. Mechanics of Materials, third ed. Prentice Hall, Upper Saddle River, NJ.

Hidayetoglu, T.K., Pica, P.N., Haworth, W.L., 1985. Aging dependence of the Bauschinger effect in aluminum alloy 2024. Mater. Sci. Eng. 73, 65–76.

Hill, R., 1948. A theory of the yielding and plastic flow of anisotropic metals. Proc. R. Soc. Lond. A 193, 281–297.

Hill, R., Hecker, S.S., Stout, M.G., 1994. An investigation of plastic flow and differential work hardening in orthotropic brass tubes under fluid pressure and axial load. Int. J. Solids Struct. 31 (21), 2999–3021.
Hollomon, J.H., 1945. Tensile deformation. Trans. AIME 162, 268–290.
Kang, G., Ohno, N., Nebu, A., 2003. Constitutive modeling of strain range dependent cyclic hardening. Int. J. Plasticity 19 (10), 1801–1819.
Karman, I., Sehitoglu, H., Chumlyakov, Y.I., Maier, H.J., 2001. The effect of twinning and slip on the Bauschinger effect of Hadfield steel single crystals. Metall. Mater. Trans. A 32 (3), 695–706.
Kotanchik, J.N., Woods, W., Weinberger, R.A., 1945. Investigation of methods of supporting single-thickness specimens in a fixture for determination of compressive stress–strain curves. National Advisory Committee on Aeronautics, Washington, DC: Wartime Report No. WR L-189. p. 19.
Kuwabara, T., Morita, Y., Miyashita, Y., Takahashi, S., 1995. Elastic–plastic behavior of sheet metal subjected to in-plane reverse loading. In: Proceedings of Plasticity '95, Dynamic Plasticity and Structural Behavior. Gordon and Breach.
LaTour, H., Wolford, D.S., 1945. Single-strip compression test for sheet materials. Proc. ASTM 45, 671–688.
Li, K.P., Carden, W.P., Wagoner, R.H., 2002. Simulation of springback. Int. J. Mech. Sci. 44 (1), 103–122.
Miller, J.A., 1944. Discussion on micro-deformation under tension and compression of thick aluminum alloy sheets for aircraft construction. Proc. ASTM 44, 569–580.
Miyauchi, K., 1984. Bauschinger Effect in Planar Shear Deformation of Sheet Metals Advanced Technology of Plasticity. Japan Society for Technology of Plasticity, Tokyo, Japan.
Moore, A.A., McDonald, J.C., 1945. Compression testing of magnesium alloy sheet. Proc. ASTM 45, 671–704.
Plumtree, A., Abdel-Raouf, H.A., 2001. Cyclic stress–strain response and substructure. Int. J. Fatigue 23, 799–805.
Ramberg, W., Miller, J.A., 1946. Determination and presentation of compressive stress–strain data for thin sheet metal. J. Aeronaut. Sci. 13 (11), 569–580.
Sandorff, P.E., Dillon, R.K., 1946. Compressive stress–strain properties of some aircraft materials. Proc. ASTM 46, 1039–1052.
Sowerby, R., Uko, D.K., Tomita, Y., 1979. A review of certain aspects of the Bauschinger effect in metals. Mater. Sci. Eng. 41 (1), 43–58.
Stoltz, R.E., Pelloux, R.M., 1976. The Bauschinger effect in precipitation strengthend aluminum alloys. Metall. Trans. A 7, 1295–1306.
Stout, M.G., Rollett, A.D., 1990. Large-strain Bauschinger effects in FCC metals and alloys. Metall. Trans. A 21 (12), 3201–3213.
Tan, Z., Magnusson, C., Persson, B., 1994. The Bauschinger effect in compression–tension of sheet materials. Mater. Sci. Eng. A 183, 31–38.
Templin, R.L., 1945. Discussion of single-strip compression test for sheet materials. Proc. ASTM 45, 690–693.
Voce, E., 1948. The relationship between stress and strain for homogeneous deformation. J. Inst. Met. 74, 537–562.
Wagoner, R.H., Chenot, J.L., 1996. Fundamentals of Metal Forming. John Wiley, New York.
Wang, J.F., Carden, W.P., Wagoner, R.H., Matlock, D.K., Barlat, F., 2004. Creep and anelasticity in the springback of aluminum. Int. J. Plasticity 20 (12), 2009–2232.
Wu, P.D., Neale, K.W., Van der Giessen, E., 1996. Simulation of the behaviour of fcc polycrystals during reversed torsion. Int. J. Plasticity 12 (9), 1199–1219.
Yaguchi, M., Takahashi, Y., 2005. Ratchetting of viscoplastic material with cyclic softening, part 1: experiments on modified 9Cr–1Mo steel. Int. J. Plasticity 21 (1), 43–65.
Yoshida, F., Uemori, T., Fujiwara, K., 2002. Elastic–plastic behavior of steel sheets under in-plane cyclic tension–compression at large strain. Int. J. Plasticity 18 (5–6), 633–659.
Zmievskii, V.I., Volkov, N.I., Pyatyshev, L.I., 1972. Device for compression testing of sheet materials. Zavodskaya Laboratoriya 38 (4), 502–503.